Computers & Structures Vol. 37, No. 6, pp. 1087–1096, 1990
Printed in Great Britain.

0045-7949/90 $3.00 + 0.00

THE USE OF THE HOFFMAN YIELD CRITERION IN FINITE ELEMENT ANALYSIS OF ANISOTROPIC COMPOSITES

J. C. J. SCHELLEKENS and R. DE BORST
Delft University of Technology, Department of Civil Engineering/TNO Institute for Building Materials and Structures, P.O. Box 5048, 2600 GA Delft, The Netherlands

(*Received* 12 *December* 1989)

Abstract—A return mapping algorithm has been developed for the Hoffman yield function of anisotropic plasticity. The accuracy of the algorithm has been assessed by means of iso-error maps for trial stress increments in the deviatoric and volumetric plane. A tangent operator that is consistent with the developed integration algorithm has been formulated. The Hoffman model has been applied to a plate structure and to two shell structures.

1. INTRODUCTION

To describe the failure behaviour of anisotropic composites a fracture criterion is needed which is able to describe the complex phenomena which govern failure in this type of materials. Criteria such as those of Tsai–Hill, Tsai–Wu and Hoffman are designed to meet this requirement.

The geometry of the Hoffman failure surface, which will be used in this investigation, is described by a quadratic function of nine independent variables which have to be determined from six uniaxial tension and compression tests and three shear tests. When the criterion is represented graphically in the principal stress space it is an elliptic paraboloid. The intersections of the limit surface with planes parallel to the deviatoric plane are ellipses, the shape of which is determined by the quadratic part of the function. The expansion of the function along its space diagonal is determined by the terms that are linear in the stress.

In this study the Hoffman criterion is used as a *yield* criterion. This implies that the calculations are not terminated after the yield surface is reached, but that they are continued in an incremental fashion. Within each loading step iterations are added to ensure that total equilibrium is complied with. In the present investigation a full Newton–Raphson method has been used. The tangential operator needed in this strategy has been derived by differentiating the stress–strain relation for finite load increments. This leads to the so-called consistent tangent matrix for anisotropic elastoplastic solids. Use of this tangential relation warrants a quadratic convergence of Newton's method.

The fully implicit Euler backward method has been applied to integrate the elasto-plastic relation. Matthies [1] has provided an elegant decomposition algorithm for use within the Euler backward scheme. In this contribution a more simple algorithm is proposed which leads to the same solution accuracy and requires an equal number of iterations to return the trial stress to the yield surface. The accuracy of the integration algorithm is assessed by iso-error maps for stress increments in both the deviatoric and the volumetric plane [2–6].

2. THE HOFFMAN YIELD CRITERION

Basically the Hoffman criterion [7] is a modification of the criterion proposed by Hill [8] through inclusion of terms that are linear in the stress. In this way the restriction of the Hill criterion, i.e. no differences between the tensile and the compressive yield strength can be described, is obviated. Hoffman originally formulated his failure criterion by the quadratic function

$$\begin{aligned} &C_1(\sigma_{22}-\sigma_{33})^2 + C_2(\sigma_{33}-\sigma_{11})^2 + C_3(\sigma_{11}-\sigma_{22})^2 \\ &\quad + C_4\sigma_{11} + C_5\sigma_{22} + C_6\sigma_{33} + C_7\sigma_{23}^2 \\ &\quad + C_8\sigma_{31}^2 + C_9\sigma_{12}^2 = 1, \end{aligned} \tag{1}$$

where the constants C_i, $i = 1, 9$, are nine independent material parameters which can be uniquely determined from six uniaxial tension and compression tests and three shear tests.

With the introduction of a yield function $\Phi(\boldsymbol{\sigma})$ the Hoffman yield criterion can be rewritten as

$$\begin{aligned} \Phi(\boldsymbol{\sigma}) = {} &\alpha_{23}(\sigma_{22}-\sigma_{33})^2 + \alpha_{31}(\sigma_{33}-\sigma_{11})^2 \\ &+ \alpha_{12}(\sigma_{11}-\sigma_{22})^2 + \alpha_{11}\sigma_{11} + \sigma_{22}\sigma_{22} \\ &+ \alpha_{33}\sigma_{33} + 3\alpha_{44}\sigma_{23}^2 + 3\alpha_{55}\sigma_{31}^2 \\ &+ 3\alpha_{66}\sigma_{12}^2 - \bar{\sigma}^2, \end{aligned} \tag{2}$$

where yielding can only occur if $\Phi = 0$. When $\bar{\sigma}_{ii}^{*}$ and $\bar{\sigma}_{ii}$ denote the compressive and tensile yield strengths in the axes of orthotropy, when $\bar{\sigma}_{ij}$ are the shear yield strengths and if $\bar{\sigma}$ is a normalised yield strength, the material parameters α_{ij} can be determined through the expressions

$$\alpha_{12} = \frac{\bar{\sigma}^2}{2}\left(\frac{1}{\bar{\sigma}_{11}^{*}\bar{\sigma}_{11}} + \frac{1}{\bar{\sigma}_{22}^{*}\bar{\sigma}_{22}} - \frac{1}{\bar{\sigma}_{33}^{*}\bar{\sigma}_{33}}\right)$$

$$\alpha_{23} = \frac{\bar{\sigma}^2}{2}\left(\frac{1}{\bar{\sigma}_{33}^{*}\bar{\sigma}_{33}} + \frac{1}{\bar{\sigma}_{22}^{*}\bar{\sigma}_{22}} - \frac{1}{\bar{\sigma}_{11}^{*}\bar{\sigma}_{11}}\right)$$

$$\alpha_{31} = \frac{\bar{\sigma}^2}{2}\left(\frac{1}{\bar{\sigma}_{11}^{*}\bar{\sigma}_{11}} + \frac{1}{\bar{\sigma}_{33}^{*}\bar{\sigma}_{33}} - \frac{1}{\bar{\sigma}_{22}^{*}\bar{\sigma}_{22}}\right)$$

$$\alpha_{11} = \bar{\sigma}^2\left(\frac{\bar{\sigma}_{11}^{*} - \bar{\sigma}_{11}}{\bar{\sigma}_{11}^{*}\bar{\sigma}_{11}}\right)$$

$$\alpha_{22} = \bar{\sigma}^2\left(\frac{\bar{\sigma}_{22}^{*} - \bar{\sigma}_{22}}{\bar{\sigma}_{22}^{*}\bar{\sigma}_{22}}\right)$$

$$\alpha_{33} = \bar{\sigma}^2\left(\frac{\bar{\sigma}_{33}^{*} - \bar{\sigma}_{33}}{\bar{\sigma}_{33}^{*}\bar{\sigma}_{33}}\right)$$

$$\alpha_{44} = \frac{\bar{\sigma}^2}{3\bar{\sigma}_{23}^2}$$

$$\alpha_{55} = \frac{\bar{\sigma}^2}{3\bar{\sigma}_{31}^2}$$

$$\alpha_{66} = \frac{\bar{\sigma}^2}{3\bar{\sigma}_{12}^2}.$$

The Hoffman yield criterion contains several other well-known yield functions as a special case. When we set $\alpha_{12} = \alpha_{23} = \alpha_{31} = \alpha_{44} = \alpha_{55} = \alpha_{66} = 1$ and $\alpha_{11} = \alpha_{22} = \alpha_{33} = 0$ the Hoffman yield function reduces to a von Mises yield function. In the principal stress space this yield contour represents a cylinder with the hydrostatic axis as the principal axis (or space diagonal). For the case that the constants α_{12}, α_{23}, α_{31}, α_{44}, α_{55} and α_{66} are not equal the Tsai–Hill yield criterion results. In the principal stress space this yield contour has the shape of an elliptic cylinder. The principal axis of this cylinder again coincides with the hydrostatic axis. The Tsai–Hill yield function is used for materials which have different strengths in the axes of orthotropy, but for which the tensile and compressive strength are equal in each direction.

If we consider the case that $\alpha_{12} = \alpha_{23} = \alpha_{31} = \alpha_{44} = \alpha_{55} = \alpha_{66} = 1$, while the parameters α_{11}, α_{22} and α_{33} are equal but nonzero, the failure surface is a cylindrical paraboloid with its space diagonal coinciding with the hydrostatic axis. The Hoffman yield function now describes a quadratic Drucker–Prager criterion.

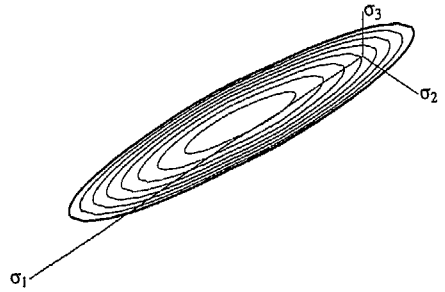

Fig. 1. Cross sections of an anisotropic Hoffman yield surface and the deviatoric plane.

In the most general case, i.e. we have neither $\alpha_{12} = \alpha_{23} = \alpha_{31} = \alpha_{44} = \alpha_{55} = \alpha_{66}$ nor $\alpha_{11} = \alpha_{22} = \alpha_{33} = 0$, the Hoffman yield function represents an elliptic paraboloid. In this case the space diagonal does not concide with the hydrostatic axis, but is merely parallel to it. The cross sections of this function with the deviatoric plane are ellipses (Fig. 1), the centres of which lie on the space diagonal.

In case of a plane–stress situation ($\sigma_{31} = \sigma_{32} = \sigma_{33} = 0$) the Hoffman criterion reduces to

$$\Phi(\boldsymbol{\sigma}) = \alpha_{23}\sigma_{22}^2 + \alpha_{31}\sigma_{11}^2 + \alpha_{12}(\sigma_{11} - \sigma_{22})^2 + \alpha_{11}\sigma_{11} + \alpha_{22}\sigma_{22} + 3\alpha_{44}\sigma_{12}^2 - \bar{\sigma}^2. \quad (3)$$

To derive the material constants for this stress situation an additional off-axis strength test is necessary to supplement the two uniaxial tests and the shear test. With $\bar{\sigma}_\theta$ the off-axis strength, the material parameters are given by

$$\alpha_{11} = \bar{\sigma}^2\left(\frac{\bar{\sigma}_{11}^{*} - \bar{\sigma}_{11}}{\bar{\sigma}_{11}^{*}\bar{\sigma}_{11}}\right)$$

$$\alpha_{22} = \bar{\sigma}^2\left(\frac{\bar{\sigma}_{22}^{*} - \bar{\sigma}_{22}}{\bar{\sigma}_{22}^{*}\bar{\sigma}_{22}}\right)$$

$$\alpha_{44} = \frac{\bar{\sigma}^2}{3\bar{\sigma}_{12}^2}$$

$$\alpha_{13} = \frac{2\bar{\sigma}^2}{\bar{\sigma}_\theta^2} + \frac{1}{2}\left(\frac{\bar{\sigma}^2}{\bar{\sigma}_{11}^{*}\bar{\sigma}_{11}} - \frac{\bar{\sigma}^2}{\bar{\sigma}_{22}^{*}\bar{\sigma}_{22}}\right) - \frac{3}{2}\alpha_{44} - \frac{(\alpha_{11} + \alpha_{22})}{\bar{\sigma}_\theta}$$

$$\alpha_{12} = \frac{\bar{\sigma}^2}{\bar{\sigma}_{11}^{*}\bar{\sigma}_{11}} - \alpha_{13}$$

$$\alpha_{23} = \frac{\bar{\sigma}^2}{\bar{\sigma}_{22}^{*}\bar{\sigma}_{22}} - \alpha_{12}.$$

For use in finite element analysis eqn (2) is better reformulated in matrix–vector notation. This results in

$$\Phi = \tfrac{1}{2}\boldsymbol{\sigma}^T\mathbf{P}_\alpha\boldsymbol{\sigma} + \boldsymbol{\sigma}^T\mathbf{p}_\alpha - \bar{\sigma}^2 \quad (4)$$

in which $\sigma^T = (\sigma_{11}, \sigma_{22}, \sigma_{33}, \sigma_{12}, \sigma_{13}, \sigma_{23})$

$$\mathbf{P}_\alpha = \begin{bmatrix} 2(\alpha_{31}+\alpha_{12}) & -2\alpha_{12} & -2\alpha_{31} & 0 & 0 & 0 \\ -2\alpha_{12} & 2(\alpha_{23}+\alpha_{12}) & -2\alpha_{23} & 0 & 0 & 0 \\ -2\alpha_{31} & -2\alpha_{23} & 2(\alpha_{31}+\alpha_{23}) & 0 & 0 & 0 \\ 0 & 0 & 0 & 6\alpha_{44} & 0 & 0 \\ 0 & 0 & 0 & 0 & 6\alpha_{55} & 0 \\ 0 & 0 & 0 & 0 & 0 & 6\alpha_{66} \end{bmatrix} \tag{5}$$

and

$$\mathbf{p}_\alpha^T = (\alpha_{11}, \alpha_{22}, \alpha_{33}, 0, 0, 0). \tag{6}$$

3. FORMULATION OF PLASTICITY RELATIONS

For perfect plasticity, to which attention is confined in this paper, the yield condition can be written in a general form as

$$\Phi(\sigma) = 0. \tag{7}$$

The time derivative of eqn (7) yields

$$\dot{\Phi}(\sigma) = \left(\frac{\partial \Phi}{\partial \sigma}\right)^T \dot{\sigma}. \tag{8}$$

The stress point must remain on the yield contour and hence $\dot{\Phi} = 0$ during yielding. According to Drucker's postulate an associative flow rule then results in

$$\dot{\epsilon}^p = \dot{\lambda} \frac{\partial \Phi}{\partial \sigma}, \tag{9}$$

where $\dot{\lambda}$ is the time derivative of the plastic multiplier, a measure of the plastic strain rate. Integrating eqn (9) gives a relation for the incremental plastic strain in a finite loading step

$$\Delta\epsilon^p = \int_t^{t+\Delta t} \dot{\lambda} \frac{\partial \Phi}{\partial \sigma} \, dt. \tag{10}$$

It is recalled that Drucker's postulate does not follow from the fundamental laws of mechanics. It is simply an assumption which must be confirmed by experimental evidence.

4. INTEGRATION OF THE ELASTO-PLASTIC RELATION

In a finite loading step the total strain increment $\Delta\epsilon$ is assumed to consist of an elastic part $\Delta\epsilon^e$ and a plastic part $\Delta\epsilon^p$

$$\Delta\epsilon = \Delta\epsilon^e + \Delta\epsilon^p. \tag{11}$$

Substituting the linear elastic stress–strain relation $\Delta\epsilon^e = \mathbf{C}\,\Delta\sigma$ in eqn (11) gives

$$-\Delta\epsilon^p = \mathbf{C}\,\Delta\sigma - \Delta\epsilon \tag{12}$$

with $\Delta\sigma$ the stress increment at the end of the loading step and $\mathbf{C}$ the elastic compliance matrix. For the incremental plastic strain it is assumed that eqn (10) can be integrated sufficiently accurately by a single-point integration rule

$$\Delta\epsilon^p = \Delta\lambda \frac{\partial \Phi}{\partial \sigma} \tag{13}$$

with $\Delta\lambda$ the finite plastic multiplier.

The derivative of $\Phi(\sigma)$ with respect to σ is given by

$$\frac{\partial \Phi}{\partial \sigma} = \mathbf{P}_\alpha \sigma + \mathbf{p}_\alpha. \tag{14}$$

When eqn (13) is rewritten with the aid of eqns (12) and (14) this results in

$$\mathbf{C}\,\Delta\sigma - \Delta\epsilon + \Delta\lambda(\mathbf{P}_\alpha(\sigma_0 + \Delta\sigma) + \mathbf{p}_\alpha) = (\mathbf{C} + \Delta\lambda\mathbf{P}_\alpha) \times (\sigma_0 + \Delta\sigma) - (\epsilon^e + \Delta\epsilon - \Delta\lambda\mathbf{p}_\alpha) = 0, \tag{15}$$

where σ_0 is the stress at the beginning of the loading step. The final stress at the end of the loading step has to be solved from this relation and is written as

$$\sigma_n = \sigma_0 + \Delta\sigma = (\mathbf{C} + \Delta\lambda\mathbf{P}_\alpha)^{-1}(\epsilon^e + \Delta\epsilon - \Delta\lambda\mathbf{p}_\alpha). \tag{16}$$

A graphical interpretation is given in Fig. 2.

Introducing eqn (16) in eqn (4) we arrive at the yield condition as a function of the plastic multiplier $\Delta\lambda$. Linearisation of the obtained relation in $\Delta\lambda$ gives ultimately

$$\Delta\lambda^{k+1} = \Delta\lambda^k - \left.\frac{\Phi}{(d\Phi/d\,\Delta\lambda)}\right|_{\Delta\lambda^k}. \tag{17}$$

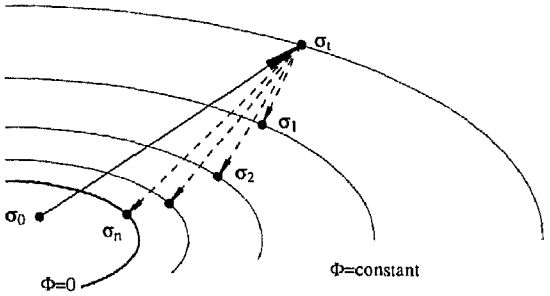

Fig. 2. Implicit Euler backward integration scheme.

To solve this relation the derivative of $\Phi(\Delta\lambda)$ with respect to $\Delta\lambda$ has to be determined

$$\frac{\partial\Phi(\Delta\lambda)}{\partial\,\Delta\lambda}=\left(\frac{\partial\Phi}{\partial\boldsymbol{\sigma}_n}\right)^T\frac{\partial\boldsymbol{\sigma}_n}{\partial\,\Delta\lambda}, \tag{18}$$

where

$$\frac{\partial\boldsymbol{\sigma}_n}{\partial\,\Delta\lambda}=-(\mathbf{C}+\Delta\lambda\mathbf{P}_\alpha)^{-1}[(\mathbf{C}+\Delta\lambda\mathbf{P}_\alpha)^{-1}\times\mathbf{P}_\alpha(\boldsymbol{\epsilon}^e+\Delta\boldsymbol{\epsilon}-\Delta\lambda\mathbf{p}_\alpha)+\mathbf{p}_\alpha]. \tag{19}$$

Substituting eqns (19) and (14) in eqn (18) yields

$$\frac{\partial\Phi(\Delta\lambda)}{\partial\,\Delta\lambda}=-(\mathbf{P}_\alpha\boldsymbol{\sigma}_n+\mathbf{p}_\alpha)^T(\mathbf{C}+\Delta\lambda\mathbf{P}_\alpha)^{-1}\times[(\mathbf{C}+\Delta\lambda\mathbf{P}_\alpha)^{-1}\mathbf{P}_\alpha(\boldsymbol{\epsilon}^e+\Delta\boldsymbol{\epsilon}-\Delta\lambda\mathbf{p}_\alpha)+\mathbf{p}_\alpha]. \tag{20}$$

The matrices $\mathbf{P}_\alpha$ and $\mathbf{C}^{-1}$ only commute for isotropic material behaviour. Then, eqn (19) can be simplified to

$$\frac{\partial\boldsymbol{\sigma}_n}{\partial\,\Delta\lambda}=-(\mathbf{C}+\Delta\lambda\mathbf{P}_\alpha)^{-1}(\mathbf{P}_\alpha\boldsymbol{\sigma}_n+\mathbf{p}_\alpha). \tag{21}$$

Substituting eqns (21) and (14) in eqn (18) now yields

$$\frac{\partial\Phi(\Delta\lambda)}{\partial\,\Delta\lambda}=-(\mathbf{P}_\alpha\boldsymbol{\sigma}_n+\mathbf{p}_\alpha)^T(\mathbf{C}+\Delta\lambda\mathbf{P}_\alpha)^{-1}\times(\mathbf{P}_\alpha\boldsymbol{\sigma}_n+\mathbf{p}_\alpha). \tag{22}$$

In an alternative approach to determine the value of the plastic multiplier $\Delta\lambda$ Matthies [1] has applied a spectral decomposition to the matrices $\mathbf{P}_\alpha$ and $\mathbf{C}$. At the expense of determining the eigenvalues of this matrix product, the matrix–vector operations in eqn (20) then do not occur and the corresponding expression in the eigenspace only involves scalar operations. Conceptually the present algorithm is more simple while giving the same accuracy and requiring an equal number of iterations.

5. CONSISTENT TANGENT OPERATOR

In nonlinear finite element analysis the stress–strain relation has to be determined within each loading step. Two different methods can be distinguished to derive this tangent relation, the classical or continuum tangent method and the consistent tangent method [9, 10]. The latter method will be described in the sequel.

The total strain at the end of iteration i is given by

$$\boldsymbol{\epsilon}^i=\boldsymbol{\epsilon}^n+\Delta\boldsymbol{\epsilon}^{i,e}+\Delta\boldsymbol{\epsilon}^{i,p}, \tag{23}$$

where $\boldsymbol{\epsilon}^n$ is the strain at the beginning of the loading step. With the relations for the incremental elastic and plastic strains

$$\Delta\boldsymbol{\epsilon}^{i,e}=\mathbf{C}(\boldsymbol{\sigma}^i-\boldsymbol{\sigma}^n) \tag{24}$$

and

$$\Delta\boldsymbol{\epsilon}^{i,p}=\Delta\lambda^i\frac{\partial\Phi}{\partial\boldsymbol{\sigma}} \tag{25}$$

the stress–strain relation can be written as

$$\boldsymbol{\epsilon}^i=\boldsymbol{\epsilon}^n+\mathbf{C}(\boldsymbol{\sigma}^i-\boldsymbol{\sigma}^n)+\Delta\lambda^i\frac{\partial\Phi}{\partial\boldsymbol{\sigma}}. \tag{26}$$

Taking the time derivative of eqn (26) results in

$$\dot{\boldsymbol{\epsilon}}^i=\mathbf{C}\dot{\boldsymbol{\sigma}}^i+\Delta\lambda^i\frac{\partial^2\Phi}{\partial\boldsymbol{\sigma}^2}\dot{\boldsymbol{\sigma}}^i+\dot{\lambda}\frac{\partial\Phi}{\partial\boldsymbol{\sigma}}. \tag{27}$$

In the case of incremental stress and strain increments the second term in the right-hand side of eqn (27) vanishes. The result is the classical, continuum elasto-plastic tangent stiffness matrix. When finite loading increments are considered this term becomes an important contribution to the elasto-plastic tangent stiffness. We now introduce a matrix $\mathbf{H}$

$$\mathbf{H}=\mathbf{C}+\Delta\lambda^i\frac{\partial^2\Phi}{\partial\boldsymbol{\sigma}^2} \tag{28}$$

so that eqn (27) can be rewritten as

$$\dot{\boldsymbol{\epsilon}}^i=\mathbf{H}\dot{\boldsymbol{\sigma}}+\dot{\lambda}\frac{\partial\Phi}{\partial\boldsymbol{\sigma}}. \tag{29}$$

Premultiplication with $\mathbf{H}^{-1}$ and $\partial\Phi/\partial\boldsymbol{\sigma}$, and invoking the consistency condition (8) yields, after some manipulations

$$\dot{\boldsymbol{\sigma}}^i=\mathbf{D}\dot{\boldsymbol{\epsilon}}^i \tag{30}$$

with

$$\mathbf{D}=\left[\mathbf{H}^{-1}-\frac{\mathbf{H}^{-1}\left(\frac{\partial\Phi}{\partial\boldsymbol{\sigma}}\right)\left(\frac{\partial\Phi}{\partial\boldsymbol{\sigma}}\right)^T\mathbf{H}^{-1}}{\left(\frac{\partial\Phi}{\partial\boldsymbol{\sigma}}\right)^T\mathbf{H}^{-1}\left(\frac{\partial\Phi}{\partial\boldsymbol{\sigma}}\right)}\right], \tag{31}$$

the so-called consistent tangent stiffness matrix. For the Hoffman yield criterion the consistent tangent matrix $\mathbf{D}$ becomes

$$\mathbf{D}=(\mathbf{C}+\Delta\lambda^i\mathbf{P}_\alpha)^{-1}-\frac{(\mathbf{C}+\Delta\lambda^i\mathbf{P}_\alpha)^{-1}(\mathbf{P}_\alpha\boldsymbol{\sigma}^i+\mathbf{p}_\alpha)\times(\mathbf{P}_\alpha\boldsymbol{\sigma}^i+\mathbf{p}_\alpha)^T(\mathbf{C}+\Delta\lambda^i\mathbf{P}_\alpha)^{-1}}{(\mathbf{P}_\alpha\boldsymbol{\sigma}^i+\mathbf{p}_\alpha)^T(\mathbf{C}+\Delta\lambda^i\mathbf{P}_\alpha)^{-1}\times(\mathbf{P}_\alpha\boldsymbol{\sigma}^i+\mathbf{p}_\alpha)}. \tag{32}$$

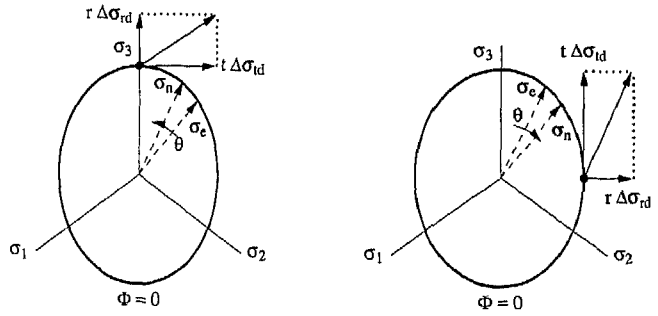

Fig. 3. Initial stress points and stress increments in the deviatoric plane.

6. ACCURACY ANALYSIS OF THE INTEGRATION ALGORITHM

The accuracy of the integration algorithm for elasto-plastic relations can be assessed by means of so-called iso-error maps [2–6]. Since the Hoffman yield criterion is dependent on the hydrostatic pressure we cannot suffice by considering the error in the deviatoric plane as with von Mises and Tsai–Hill plasticity, but we also have to consider errors in the volumetric direction. At this point some explanation is in order with respect to the definition of radial and tangential trial stress increments both in the deviatoric and in the volumetric plane and on the location of the initial stress points (see Figs 3 and 4). We define the deviatoric plane as $\sigma_{11}+\sigma_{22}+\sigma_{33}=0$. If we consider anisotropic material properties the cross-section of the yield surface and the deviatoric plane is elliptically shaped. The initial stress points are the intersections of the ellipse with its principal axes, i.e. the points of smallest and strongest curvature. The line connecting the initial stress point with the centre of the ellipse is the normal vector of the volumetric plane.

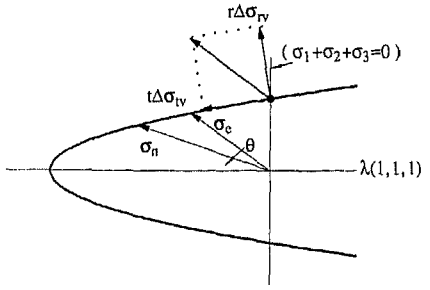

Fig. 4. Stress increments in the volumetric plane.

In the deviatoric plane the radial trial stress increment $\Delta\sigma_{rd}$ is directed normal to the yield surface whereas the direction of the tangential trial stress increment $\Delta\sigma_{td}$ is along the yield surface. The same holds for radial and tangential stress increments $\Delta\sigma_{rv}$ and $\Delta\sigma_{tv}$ in the volumetric plane. For the radial and tangential stress increments in the deviatoric plane ($\Delta\sigma_{rd}$ and $\Delta\sigma_{td}$) the unit magnitude is defined to be equal to a stress increment which, starting from a stress-free state, induces initial yielding in the corresponding direction. For material 1, which represents an isotropic Hoffman yield contour (Table 1), the unit magnitude of the radial stress increment in the volumetric plane $\Delta\sigma_{rv}$ is defined in a similar fashion. The unit magnitude of the radial stress increment for materials 2, 3, and 4 (Table 1) is equal to $\Delta\sigma_{rv}$ of material 1. The unit magnitude of the tangential stress increment $\Delta\sigma_{tv}$ is equal to $\Delta\sigma_{rv}$ for all four sets of material constants.

Incrementing the trial stress in the deviatoric plane results in a component of the final stress increment not only in the deviatoric plane, but also in the volumetric plane. Therefore we define θ_d as the angle between projections of the exact stress σ_e and numerically determined stress σ_n on the deviatoric plane and θ_v as the angle between projections on the volumetric plane. The angles are positive for the directions as given in Figs 3 and 4. The error in the norm of σ_n is defined as

$$\text{error} = \frac{\sqrt{((\sigma_e-\sigma_n)^T(\sigma_e-\sigma_n))}}{\sqrt{(\sigma_e^T\sigma_e)}} \times 100\%. \quad (33)$$

Table 1. Material sets for error maps

	$\bar{\sigma}_{11}^*$	$\bar{\sigma}_{11}$	$\bar{\sigma}_{22}^*$	$\bar{\sigma}_{22}$	$\bar{\sigma}_{33}^*$	$\bar{\sigma}_{33}$
Mat. 1	1.0E4	1.0E3	1.0E4	1.0E3	1.0E4	1.0E3
Mat. 2	5.0E3	1.0E3	1.0E3	1.0E3	1.0E3	1.0E3
Mat. 3	1.0E4	1.0E3	1.0E3	1.0E3	1.0E3	1.0E3
Mat. 4	2.0E4	1.0E3	1.0E3	1.0E3	1.0E3	1.0E3
	α_{11}	α_{22}	α_{33}	α_{12}	α_{13}	α_{23}
Mat. 1	9.0E2	9.0E2	9.0E2	0.05	0.05	0.05
Mat. 2	8.0E2	0.0	0.0	0.1	0.1	0.90
Mat. 3	9.0E2	0.0	0.0	0.05	0.05	0.95
Mat. 4	9.5E2	0.0	0.0	0.025	0.025	0.975

Note that the 'exact' stress is computed by subdividing the applied stress increment into 1000 subincrements.

For the sets of material parameters from Table 1, iso-error maps have been computed. The results are given in Figs 5–8. Material 1 represents an isotropic Hoffman yield function with the compressive yield strength 10 times the tensile yield strength. An anisotropic yield function governs the plastic behaviour of materials 2, 3 and 4, for which the compressive yield strength in one axis of orthotropy is respectively five, 10 and 20 times the compres-

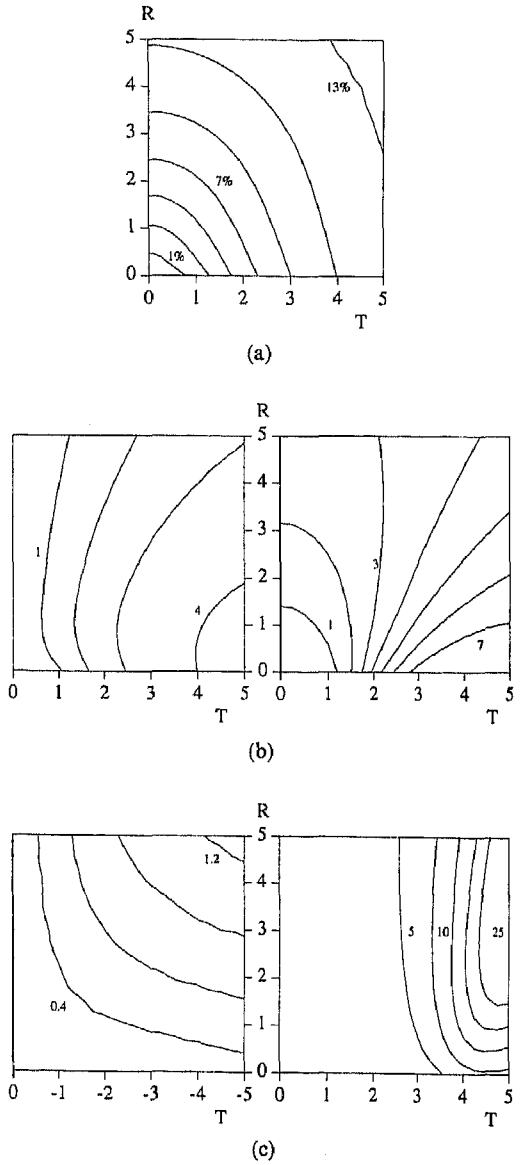

Fig. 5. Iso-error maps of material 1. (a) Errors in norms of numerically determined stresses (stress increments in the deviatoric plane); (b) angles between exact and numerically determined stresses (stress increments in the deviatoric plane), *left*: θ_d, *right*: θ_v; (c) angles between exact and numerically determined stresses (stress increments in the volumetric plane), *left*: $\Delta\sigma_{tv}$ in negative direction, *right*: $\Delta\sigma_{tv}$ in positive direction.

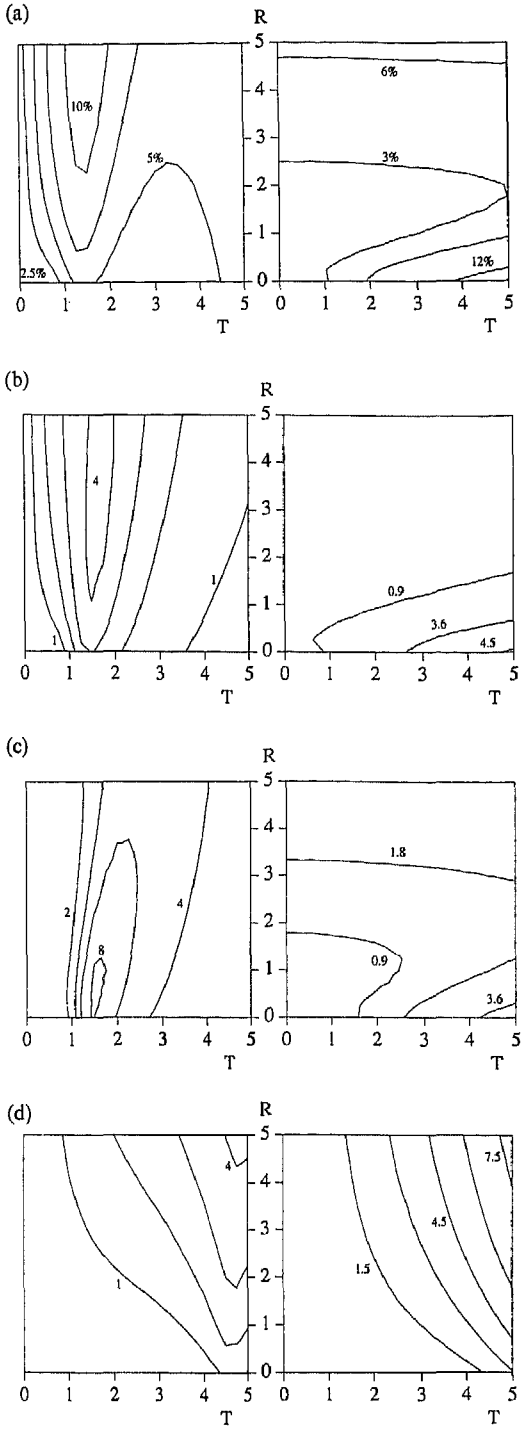

Fig. 6. Iso-error maps of material 2. (a) Errors in norms of numerically determined stresses (stress increments in the deviatoric plane), *left*: point of smallest curvature, *right*: point of strongest curvature; (b) angles θ_d between exact and numerically determined stresses (stress increments in the deviatoric plane), *left*: point of smallest curvature, *right*: point of strongest curvature; (c) angles θ_v between exact and numerically determined stresses (stress increments in the deviatoric plane), *left*: point of smallest curvature, *right*: point of strongest curvature; (d) angles between exact and numerically determined stresses (stress increments $\Delta\sigma_{tv}$ in the volumetric plane, positive direction), *left*: point of smallest curvature, *right*: point of strongest curvature.

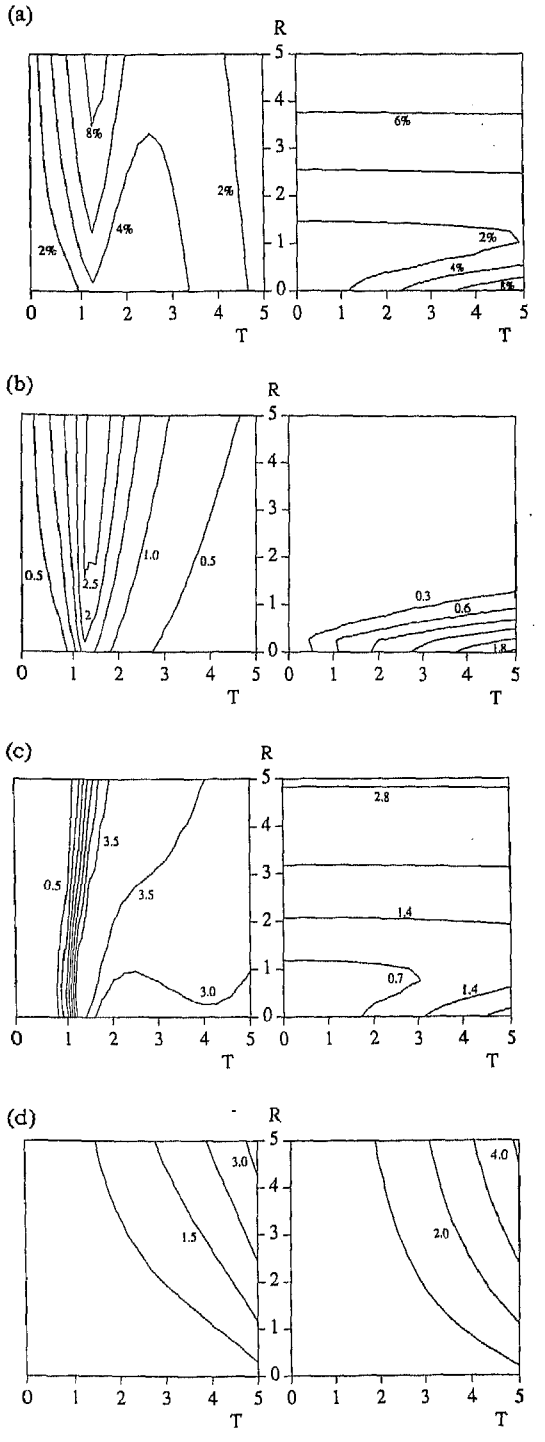

Fig. 7. Iso-error maps of material 3. (a) Errors in norms of numerically determined stresses (stress increments in the deviatoric plane), *left*: point of smallest curvature, *right*: point of strongest curvature; (b) angles θ_d between exact and numerically determined stresses (stress increments in the deviatoric plane), *left*: point of smallest curvature, *right*: point of strongest curvature; (c) angles θ_v between exact and numerically determined stresses (stress increments in the deviatoric plane), *left*: point of smallest curvature, *right*: point of strongest curvature; (d) angles between exact and numerically determined stresses (stress increments $\Delta\sigma_w$ in the volumetric plane, positive direction), *left*: point of smallest curvature, *right*: point of strongest curvature.

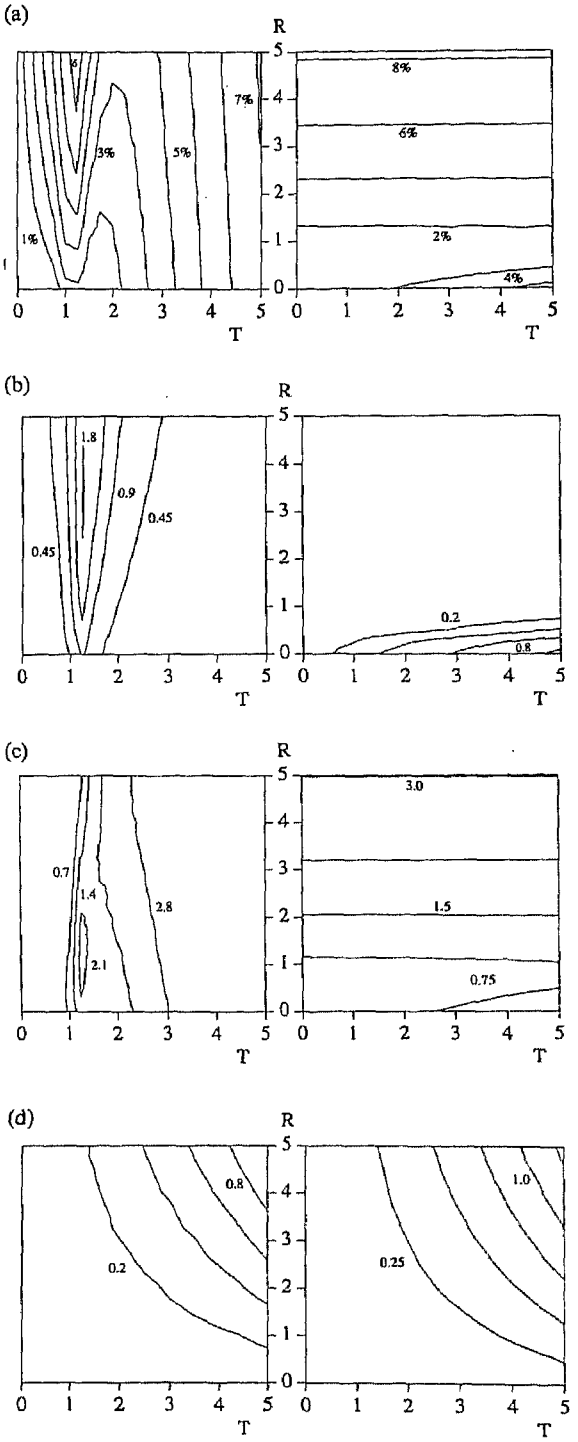

Fig. 8. Iso-error maps of material 4. (a) Errors in norms of numerically determined stresses (stress increments in the deviatoric plane); *left*: point of smallest curvature, *right*: point of strongest curvature; (b) angles θ_d between exact and numerically determined stresses (stress increments in the deviatoric plane), *left*: point of smallest curvature, *right*: point of strongest curvature; (c) angles θ_v between exact and numerically determined stresses (stress increments in the deviatoric plane), *left*: point of smallest curvature, *right*: point of strongest curvature; (d) angles between exact and numerically determined stresses (stress increments $\Delta\sigma_w$ in the volumetric plane, positive direction), *left*: point of smallest curvature, *right*: point of strongest curvature.

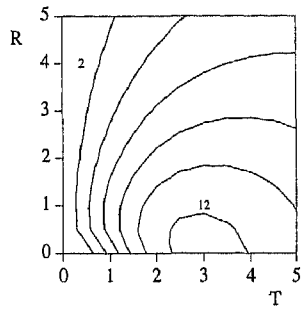

Fig. 9. Iso-error map for the von Mises yield function.

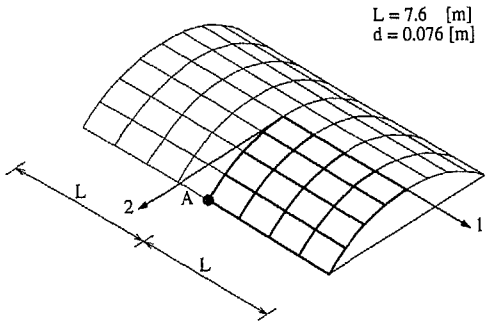

Fig. 10. Geometry of the cylindrical shell.

sive yield strength in other axes of orthotropy. In the computations the tangential trial stress in the volumetric planes ranges from -5 to 5 times the unit magnitude with positive direction towards the apex of the yield surface. The magnitude of all other trial stress increments is between 0 and 5 times the unit increment. In Figs 5–8 R and T are the multipliers for the radial and tangential unit trial stress increments.

On basis of the iso-error maps the following remarks can be made:

- When the anisotropy of the yield surface becomes more pronounced, the errors in numerical results decrease. Taking into account the fact that use of implicit integration at corners in the yield surface leads to exact results [11], the observed tendencies of decreasing errors at points with a strong curvature are well explainable.
- The calculated errors are small when compared to the von Mises criterion (Fig. 9). Only when the tangential trial stress increment $\Delta\sigma_{t0}$ is directed towards the apex of the yield surface, do the errors become relatively large, especially when the trial stress is beyond the apex (Fig. 5c).
- When the trial stress is in the volumetric plane and directed from the apex, the errors are small. For this reason the corresponding iso-error map is only given for material 1 (Fig. 5c).
- Figure 6c and f show that the errors belonging to the point of strongest curvature in the deviatoric plane exceed the errors belonging to the point of smallest curvature in the deviatoric plane when the trial stress increments are in the volumetric direction. This is because points of the yield contour where the curvature in the deviatoric plane is large show a smaller curvature in the volumetric plane than points that have a small curvature in the deviatoric plane.
- If an initial stress point is located at the strongly curved part of the yield surface and the trial stress increment is in the deviatoric plane, we note that for large σ_r/σ_t ratios the errors become less dependent on the tangential stress increments when a material becomes more anisotropic. We also observe that the errors θ_v in the volumetric direction slightly increase with increasing anisotropy. This is a result of a decreasing curvature of the yield surface in the volumetric direction.

7. EXAMPLES

All the example calculations to be discussed in the sequel have been carried out under arc-length control and a full Newton–Raphson iteration method has been used. Since the use of the consistent tangent operator leads to improved convergence behaviour when compared to the continuum tangent operator, especially when anisotropic material properties are concerned [12], calculations have been carried out with the former method.

A cylindrical shell

The first shell structure that has been analysed is the cylindrical shell of Fig. 10 [13, 14]. The vertical displacements of both curved ends are prevented. Because of symmetry considerations the calculations have been carried out for only a quarter of the shell. Eight-noded degenerated shell elements with 2×2 Gauss integration in the plane and a five-point Simpson integration through the thickness have been used. In the calculations a Young's modulus of $E = 21 \times 10^6\ \mathrm{kN/m^2}$ and a Poisson's ratio $\nu = 0$ have been used. The yield stresses used in the analyses are given in Table 2. Figure 11 shows the load–deflection curves for the different cases under a uniformly distributed self-weight load.

Table 2. Plastic material properties

	$\bar{\sigma}_{11}$	$\bar{\sigma}^*_{11}$	$\bar{\sigma}_{22}$	$\bar{\sigma}^*_{22}$	$\bar{\sigma}_{33}$	$\bar{\sigma}^*_{33}$	$\bar{\sigma}_{12}$	$\bar{\sigma}_{13}$	$\bar{\sigma}_{23}$
Case 1	4.2E3	4.2E3	4.2E3	4.2E3	4.2E3	4.2E3	2.4E3	2.4E3	2.4E3
Case 2	4.2E3	8.4E3	4.2E3	8.4E3	4.2E3	8.4E3	2.4E3	2.4E3	2.4E3
Case 3	8.4E3	4.2E3	8.4E3	4.2E3	8.4E3	4.2E3	2.4E3	2.4E3	2.4E3
Case 4	4.3E4	4.3E3	4.3E3	4.3E3	4.3E3	4.3E3	2.4E3	2.4E3	2.4E3

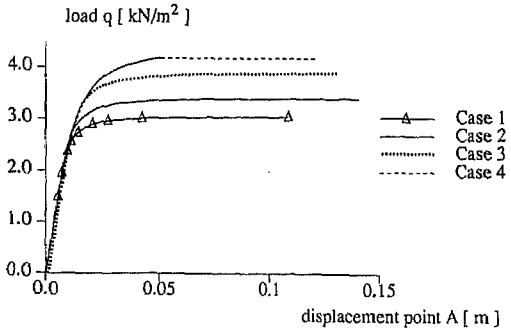

Fig. 11. Load–deflection curves for point A.

A clamped plate

The second example concerns a clamped square plate which is loaded in the centre by a concentrated load [13, 14]. Again, only a quarter of the plate has been modelled because of symmetry considerations (Fig. 12). The same elements have been used as in the first example with 2×2 integration in the plane and seven integration points through the thickness. Analyses have been carried out with a Young's modulus $E = 30 \times 10^6\ \mathrm{kN/m^2}$ and a Poisson's ratio $\nu = 0.3$. The yield values are given in Table 3. The hardening behaviour has been modelled by using Besseling's fraction model [15]. The hardening modulus of $h = 0.01E$ has been approximated by a two-fraction model with weights $\phi_1 = 0.99$ and $\phi_2 = 0.01$ where the second fraction remains elastic throughout the loading process. Figure 13 shows the load as a function of the displacement of the centre of the plate for the case listed in Table 3.

A spherical shell

The third example is the clamped spherical shell of Fig. 14 [12, 13]. The material properties are identical to those of the clamped plate. Again only a quarter of the structure has been analysed. The shell is loaded in the centre by a concentrated load. The number of integration points is as in the second example. Figure 15 shows the load in the centre of the shell as a function of the vertical displacement in that point for the various cases.

From Figs 11, 13 and 15 we observe that a clear difference exists between the results for the isotropic and the anisotropic strength properties. In cases of anisotropy the ultimate bearing capacity increases up to 100%. Because of the arching effect, an increase of the compressive yield strength has a greater influence on the bearing capacity of the two shells than has an

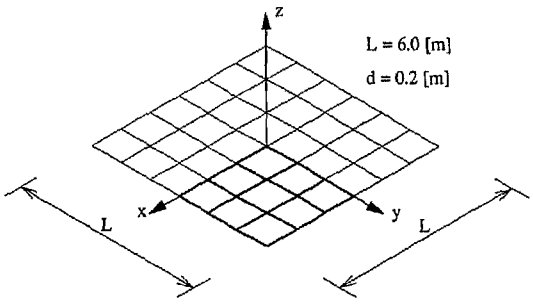

Fig. 12. Geometry of the clamped plate.

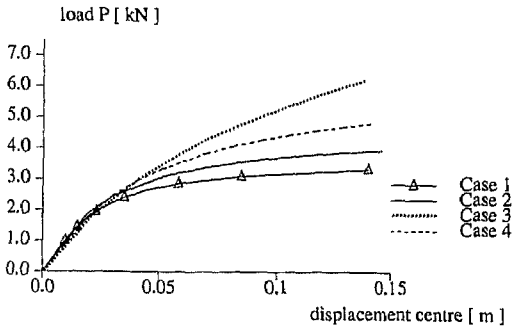

Fig. 13. Load–deflection curves for the centre of the plate.

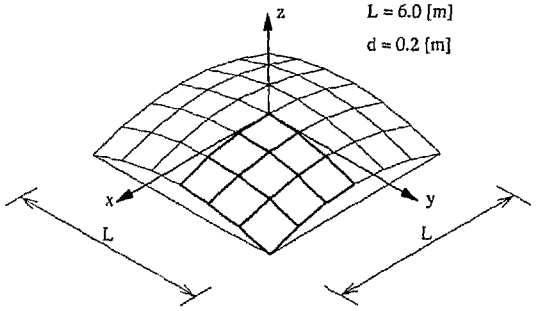

Fig. 14. Geometry of a clamped spherical shell.

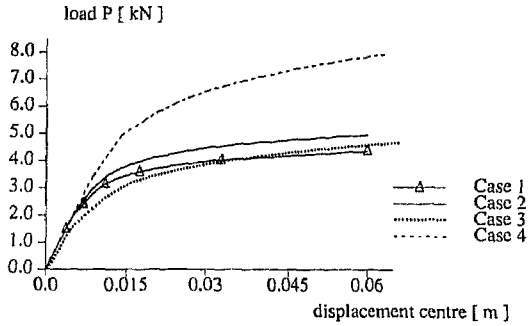

Fig. 15. Load–deflection curves for the centre of the spherical shell.

Table 3. Material properties for plastic behaviour

	$\bar{\sigma}_{11}$	$\bar{\sigma}^*_{11}$	$\bar{\sigma}_{22}$	$\bar{\sigma}^*_{22}$	$\bar{\sigma}_{33}$	$\bar{\sigma}^*_{33}$	$\bar{\sigma}_{12}$	$\bar{\sigma}_{13}$	$\bar{\sigma}_{23}$
Case 1	3E4	3E4	3E4	3E4	3E4	3E4	1.7E4	1.7E4	1.7E4
Case 2	3E4	3E4	4E4	4E4	3.5E4‡	—	2.02E4	1.7E4	1.7E4
Case 3	6E4	3E4	6E4	3E4	6E4	3E4	1.7E4	1.7E4	1.7E4
Case 4	6E4	3E4	6E4	3E4	6E4	3E4	1.7E4	1.7E4	1.7E4

‡ The value of $\bar{\sigma}_{45}$ is given.

increase of the tensile yield strength. For the plate structure the opposite holds true.

8. CONCLUDING REMARKS

In this contribution an Euler backward algorithm has been derived and assessed for the Hoffman yield criterion of anisotropic plasticity. The algorithm appeared to be accurate even for strongly curved parts of the yield contour. This appeared to hold true for the errors in the deviatoric plane as well as those in the volumetric plane. Only when the trial stress increments in the volumetric plane are directed towards the apex, do larger deviations from the exact solution occur. The fact that the Euler backward algorithm yields only small to moderate errors for the Hoffman yield criterion gives confidence that application of this algorithm to more sophisticated anisotropic yield functions (e.g. Tsai and Wu [16] where we have coupling between shear and normal stress components) also results in an acceptable accuracy.

Acknowledgement—The calculations presented in this paper have been carried out with the finite element package DIANA of the TNO Institute for Building Materials and Structures.

REFERENCES

1. H. G. Matthies, A decomposition method for the integration of the elastic-plastic rate problem. *Int. J. Numer. Meth. Engng* **28,** 1–11 (1989).
2. R. D. Krieg and D. B. Krieg, Accuracies of numerical solution methods for the elastic–perfectly plastic model. *J. Press. Vessel Technol.* **99,** 510–515 (1977).
3. H. L. Schreyer, R. F. Kulak and J. M. Kramer, Accurate numerical solution for elasto-plastic models. *J. Press. Vessel Technol.* **101,** 226–234 (1979).
4. M. Ortiz and E. P. Popov, Accuracy and stability of integration algorithms for elastoplastic constitutive relations. *Int. J. Numer. Meth. Engng* **21,** 1561–1576 (1985).
5. M. Ortiz and J. C. Simo, An analysis of a new class of integration algorithms for elastoplastic constitutive relations. *Int. J. Numer. Meth. Engng* **23,** 353–366 (1986).
6. J. C. Simo and R. L. Taylor, A return mapping algorithm for plane stress elasto-plasticity. *Int. J. Numer. Meth. Engng* **22,** 649–670 (1986).
7. O. Hoffman, The brittle strength of orthotropic materials. *J. Comp. Mater.* **1,** 200–206 (1967).
8. R. Hill, A theory of the yielding and plastic flow of anisotropic materials. *Proc. R. Soc.* **A193,** 281–297 (1947).
9. J. C. Simo and R. L. Taylor, Consistent tangent operators for rate-independent elasto-plasticity. *Comput. Meth. appl. Mech. Engng* **48,** 101–118 (1985).
10. E. Ramm and A. Matzenmiller, Computational aspects of elasto-plasticity in shell analysis. In *Proceedings of the International Conference on Computational Plasticity* (Edited by D. R. J. Owen, E. Hinton and E. Onate), pp. 711–735. Pineridge Press, Swansea (1987).
11. R. de Borst, Integration of plasticity equations for singular yield functions. *Comput. Struct.* **26,** 823–829 (1987).
12. R. de Borst and P. H. Feenstra, Studies in anisotropic plasticity with reference to the Hill criterion. *Int. J. Numer. Meth. Engng* **29,** 315–336 (1990).
13. D. R. J. Owen and J. A. Figueiras, Elasto-plastic analysis of anisotropic plates and shells by the semi-loof element. *Int. J. Numer. Meth. Engng* **19,** 521–539 (1983).
14. D. R. J. Owen and J. A. Figueiras, Anisotropic elasto-plastic finite element analysis of thick and thin plates and shells. *Int. J. Numer. Meth. Engng* **19,** 541–566 (1983).
15. J. F. Besseling, A theory of elastic, plastic and creep deformations of an initially isotropic material showing anisotropic strain-hardening, creep recovery and secondary creep. *J. appl. Mech.* **25,** 529–536 (1958).
16. S. W. Tsai and E. M. Wu, A general theory of strength of anisotropic material. *J. Comp. Mater.* **5,** 58–80 (1971).